Journal of Radiation and Nuclear Applications
An International Journal

http://dx.doi.org/10.18576/jrna/020303

A Combination of μ-PIXE, XRF, SEM-EDS and XRD Techniques in the Analyses of Sn-Mine Tailings

Felix S. Olise[1,*], *Oyediran K. Owoade*[1], *Solomon A. Adekola*[2], *Hezekiah B. Olaniyi*[1],*Christopher B. Mtshali*[3], *Wojciech J. Przybylowicz*[3, 4], *Carlos A. Pineda-Vargas*[3, 5] *and Malik Maaza*[3]

[1]Department of Physics and Engineering Physics, Obafemi Awolowo University, Ile-Ife, Nigeria.
[2]Department of Geology, Obafemi Awolowo University, Ile-Ife, Nigeria.
[3]Materials Research Department, iThemba LABS, National Research Foundation, P.O. Box 722, Somerset West 7129, South Africa.
[4]AGH University of Science and Technology, Faculty of Physics & Applied Computer Science, Al. A. Mickiewicza 30, 30-059 Krakow, Poland.
[5]Faculty of Health and Wellness Sciences, CPUT, Bellville, South Africa.

Received: 6 Jun. 2017, Revised: 20 Aug.2017, Accepted: 25 Aug. 2017.
Published online: 1 Sep. 2017.

Abstract: A combination of microprobe proton induced x-ray emission (μ-PIXE), x-ray fluorescence (XRF), energy dispersive spectroscopy-scanning electron microscopy (SEM-EDS) and x-ray diffraction (XRD) techniques have been applied in the analyses of tailings of tin (Sn) mining activities in the Jos Plateau, Nigeria. This paper reviews the elemental composition and distribution maps across single mineral grains. The microscopic data obtained are discussed to understand the mineral phases; and the provenance of economically important recoverable metals, associated with the major indicator mineral element, contained in the investigated samples. Caution is required when using automated elemental analysis of the portable XRF instrument, of which user has no control. The obtained results must always be confirmed using another analytical method.

Keywords: Indicator Mineral, micro-PIXE, XRF, SEM-EDS, Phases.

1 Introduction

Characterisation of tin reserves in terms of its mineral makeup has indicated cassiterite as its major occurrence. Other minerals include but not limited to tin sulphides, stannite and kieserite [1]. Amongst the ore phases, the sulphides and pyrite showed consistent behavioural similarity during the various stages of mineral beneficiation. The major recovery processes are through flotation, gravity concentration and magnetic separation [2]. The recovery processes, using the above methods, have proved inefficient and consistently resulted in poor concentrate grade [3]. This has necessitated the development of efficient and cost-effective processing procedures [2, 4, 5]. The mineral extraction process is challenging because the main mineral – cassiterite – is fragile and can be easily lost to grinding [6, 7].Also, the fine nature of the grain size of the main mineral and its distribution in the ore makes the beneficiation process a difficult exercise.Tin, because of its high developmental importance [8], requires sufficient characterization of its ore, which is central to process selection. In addition, there are other economically important metals, which could be present in commercial quantities and recoverable. Also, the governmental efforts in the area of mineral mapping and remediation of the abandoned tin in younger granites and other similar basement complex rocks mines, in Nigeria, should be adequately coordinated.In this work, the complementarity of multi-analytical techniques comprising micro-particle induced x-ray emission (μ-PIXE) spectroscopy, x-ray fluorescence (XRF) spectroscopy, scanning electron microscopy revolved around energy-dispersive spectroscopy (SEM-EDS) and x-ray diffraction spectroscopy (XRD) are combined in characterizing tin mine tailings for the major and associated mineral make-up. While we first examined the qualitative assessment of the

*Corresponding author e-mail: felixolise49@gmail.com

samples by XRF and SEM-EDS, the characteristic merits and drawbacks of each technique was taken into consideration for optimization purposes. The μ-PIXE procedure eliminates the use of standard materials, which presents poor representation of the natural material and the complex geometries of the heterogeneous geological samples. The incident protons-produced bremsstrahlung background in μ-PIXE is far less than in EDS-SEM due to incident electrons [9]. As such, μ-PIXE has the advantage of trace element measurements necessary to extract essential geological data regarding activities that abound in the ores and, by extension, in prospecting for minerals and metals that are economically significant. The EDS-SEM was used to obtain the major elemental concentrations [10], and together with the other techniques, we present the qualitative and quantitative data generated in connection to the phases, elemental imaging as well as fingerprinting of the samples.

2 Materials and Methods

2.1 Geology of the Study Area and Sampling Information

The detailed studies of the Younger Granites have been carried out in Nigeria, partly for their intrinsic interest. Comparatively, this has provided data in studying similar geological formations worldwide. Since 1900s, Younger Granites have been acknowledged as the reservoir of fertile alluvial tin (cassiterite) sediments that had been agelong known to exist around the Jos Plateau in association with biotite granite [11].

The tin mine tailings for this study were obtained from the three old mines in Bisichi, Kuru and Bukuru regions, Jos Plateau, Nigeria and the provenience of selected samples are presented in Table 1. The cottage-like processing companies, situated amongst areas of human settlement, depend on the mine tailings and seldomly virgin heap of sediments from the mining sites for their activities. Twenty collected samples were air dried to constant weights at the laboratory. The detailed description of the study area, map as well as the sampling procedure can be found in [12].

2.2 High Resolution Scanning Electron Microscope (HRSEM) and Energy Dispersive Spectroscopy (EDS)

The electron microscope with its high resolution scanning power (HRSEM) and equipped with a detector of energy dispersive capacity was used in the investigation of morphology and elemental composition in various areas of the selected samples. All samples were homogenized and pelletised using a pellet press operated under vacuum. Thin(~100 Å in thickness) layer of carbon was deposited on front surfaces of all pelletised samples using high quality compact desktop vacuum coating system. This was for conductivity enhancement and charge build-up prevention, ensuring good image detail and clarity. Carbon coating enables good atomic number contrast, without additional spurious x-ray peaks and with minimal increase of absorption of low-energy x-rays from the samples [13, 14]. The samples were fitted into the vacuum chamber of the high-resolution scanning electron microscope (HRSEM, Auriga Zeiss Ultra 55 Field Emission) with In-lens detection real-time of 21-36 seconds, live time of 60 seconds and resolution of 1 nm. Images were recorded at electron beam accelerating voltage and current of 30 kV and 10 nA, respectively. EDS spectra were recorded using energy dispersive spectrometry (EDS) with the hyper-thin window located inside the HRSEM while the back scattering electron detectors were used to acquire the images.

Table 1. Provenience of selected samples.

Sample	Geographical location	Mine	Location in the mine
D1	Jos Plateau	Bisichi	Outside
B2	Jos Plateau	Kuru	Inside
A1	Jos Plateau	Bukuru	Processing area
B1	Jos Plateau	Bukuru	Processing area

2.3 X-ray Powder Diffraction (XRD)

Each of the samples was examined by powder x-ray diffraction (XRD) for crystal phase information. The samples were laid in a Lucite holder on the goniometer of the Brucker-D8 advance GER x-ray diffractometer using Cu-Kα irradiation (wavelength, λ = 1.5406 Å), at the Materials Research Department (MRD), iThemba LABS, Somerset West, South Africa. The XRD operating voltage was 40 kV and current was 300 mA; with step size of 0.034º to make x- ray patterns with adequate intensity to create lines to determine the minerals at the 2θ angles (8.000º – 90.016º). The mineral phases were identified using the Joint Committee on Powder Diffraction Standard (JCPDS) software, JCPDFWIN.

2.4 X-ray Fluorescence Spectroscopy

Samples in the powder form, contained in the plastic bags, were analysed using the portable Thermo Scientific Niton (Model: XL3t-77736) XRF analyzer. The mining

operational mode was used with energy range of 0-56 keV and a counting time of 60 seconds. The instrument was brought close to the samples, but avoiding contacts, at constant geometry. In addition to the automatic analysis of elemental composition, raw x-ray spectra were also stored in four energy ranges (main range, light range, low range and high range).

2.5 Proton Induced X-ray Emission (PIXE) Spectrometry

Elemental analysis of the samples was carried out using PIXE along with the proton elastic back-scattering (EBS) available at the nuclear microprobe facility, MRD, iThemba LABS, Somerset West, South Africa. The homogenized samples were pelletised into sizes of about one cm in diameter. The measurement of the samples were carried out with a 3 MeV proton beam generated by a 6 MV single-ended Van de Graaff accelerator. The Oxford magnetic quadrupole triplet (OM 150) was used for beam focusing to a 5 x 5 μm^2 spot. The beam current was kept between 100 to 200 pA in order to bring the PIXE spectra pileups to a minimum and square or rectangular scan patterns over selected areas of samples were raster scanned, using variable sizes of the order of 1 mm x 1 mm.
PIXE spectra were recorded between 1 and 44 keV x-ray energy range using a Si(Li) detector, placed at a take-off angle of 135^0 with effective energy resolution (for the Mn K-alpha line) of about 160 eV. Data acquisition was performed in the case-by-case mode using CAMAC and VME bus modules and XSYS software running on a VAX-4000 computer. For the control of specimen stage stepper motors, magnetic scanning coils and the beam-on-demand deflection coils, the system was linked with a PC running programs written in Lab VIEW. Integrated beam charge was collected from the insulated specimen holder and used to normalize the results. The 125 μ m thick Be absorber was injected between the sample and detector in order to shield the detector from scattered protons. Quantitative results of the analysis were obtained by employing the no-standard method using Geo PIXE II software [15]. The elemental mapping of the samples was thereafter carried out by applying the dynamic analysis technique [16]. An annular Si surface barrier detector, which was placed at a mean angle of $176^0$was used in obtaining the proton elastic backscattering (EBS) spectra. But the results are not reported here.

3 Results

3.1 Morphology and Mineral phases: XRD and SEM

The results of XRD and SEM-EDS analyses provided information on the ore phases, giving visual data and enabling more holistic mineralization information. XRD revealed the presence of the following mineral phases: quartz, ilmenite, zircon, tin selenide, iron niobium oxide, zirconium hydride, iron silicate hydroxide, baumite and kaolinite (Table 2). Figure 1 shows an example of SEM image (sample D1) with various mineral phases identified. It also illustrates high level of inhomogeneity of samples. EDX spectra collected from places selected within scanned areas showed presence of Al, Si, K, Ca, Ti, Fe, Cu, Zn, As, Zr, Sn, W, Th and U. The association of these elements with four major mineral phases - Quartz and Zircon ($ZrSiO_4$) was already reported earlier [17]. The additional phases, Ilmenite ($FeTiO_3$) and Tin Selenide (SnSe), might, therefore, justifies the improved beneficiation methods in the event of the minerals availability in commercial quantities and recoverable forms in the original ore.

Table 2. Identification of mineral phases from XRD analysis.

Sample	Mine	Mineral phases
D1	Bisichi	Quartz SiO_2 Ilmenite $FeTiO_3$ Zircon $ZrSiO_4$ Tin Selenide SnSe
B2	Kuru	Zircon $ZrSiO_4$ Iron Niobium Oxide $Fe(NbO_3)_2$ Zirconium hydride epsilon-ZrH_2
A1	Bukuru	Quartz SiO_2 Iron Silicate Hydroxide $Fe_3Si_2O_5(OH)_4$ Baumite $(Mg,Mn,Fe,Zn)_3(Si,Al)_2O_5(OH)_4$
B1	Bukuru	Quartz SiO_2 Kaolinite $Al_2Si_2O_5(OH)_4$

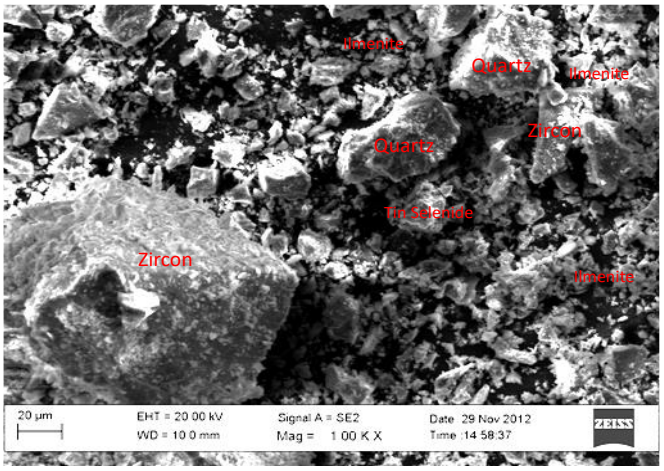

Figure 1. SEM image of sample D1 showing distribution of mineral phases and high level of in homogeneity.

3.2 XRF and PIXE

The results of automated analysis of XRF spectra for the four selected samples out of twenty are shown in Table 3, while the raw spectra of two samples (A1 and B2) are shown in Figures 2 and 3, respectively. The calculation algorithm used assumes that the concentrations of detected elements should add up to 100%, without taking into account the not-detectable light elements, especially oxygen. PIXE results are calculated without such assumption.

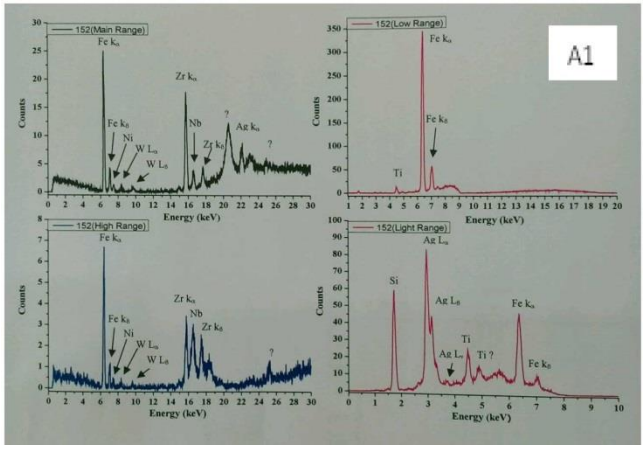

Figure 2. XRF spectra of sample A1. Note the presence of Ti peaks and absence of Ba peaks.

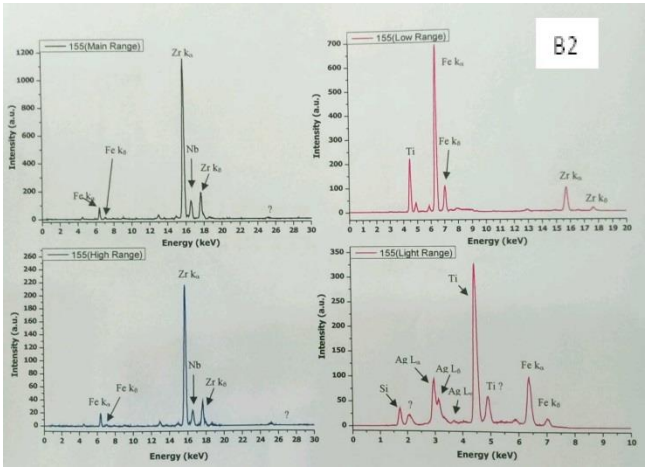

Figure 3. XRF spectra of sample B2. Note the presence of Ti peaks and absence of Ba peaks.

Sample A1. XRF identified Al, Si, Cl, Fe, Y, Zr, Nb, Ba, REEs (Ce, Pr, Nd), W and Th (Table 3). Barium concentration exceeds 80% and, according to the results of automated analyses, it should be the dominating element in the x-ray spectra. However, visual inspection of the respective spectrum (Fig. 2) does not reveal the presence of barium x-ray lines. On the other hand, the Ti K-lines are easily identifiable. Titanium, according to the results in Table 3, is below the limit of detection and the error of analysis is high (1.306 wt.%).

PIXE identified the presence of Al, Si, S, K. Ca, Ti, Cr, Fe, Zr and W (Table 4). All elements were analysed on K-lines with the exception of tungsten, analysed on L-lines.

Sample B1. XRF identified Al, Si, Fe, Sr, Y, Zr, Nb, Mo, Sn, Ba, REEs (La, Ce, Pr, Nd), Pb and Th (Table 3). Barium concentration is of the order of 86%. However, visual inspection of the respective spectrum (not shown) does not reveal the presence of barium x-ray lines. Titanium, according to the results from Table 3, is below the limit of detection and the error of analysis is high (2.713 wt%).

PIXE identified the presence of Al, Si, P, K, Ca, Ti, Cr, Mn, Fe, Ni, Zn, Y, Zr, Nb and Hf (Table 4). All elements were analysed on K-lines with the exception of hafnium, analysed on L-lines. Ti concentration was much higher than in sample A1, exceeding 0.7 wt%.

Sample B2. XRF identified Al, Si, Mn, Fe, Ni, Cu, Zn, As, Y, Zr, Nb, Mo, Sn, Ba, REEs (La, Ce), W, Pb, Bi, Th and U (Table 3). Barium concentration is of the order of 59%. However, visual inspection of the respective spectrum (Fig. 3) does not reveal the presence of barium x-ray lines. Titanium, according to the results from Table 3, is below the limit of detection and the error of analysis is very high (~ 13.8 wt%).

PIXE identified the presence of Al, Si, P, S, Ca, Ti, Cr, Mn, Fe, Zn, Y, Zr, Nb, Sn, Yb, Hf, Ta, Pt, Au, Th and U (Table 4). Ti concentration was above 4 wt%.

Sample D1. XRF identified Al, Si, Cl, Mn, Fe, Ni, Cu, Zn, Y, Zr, Nb, Mo, Sn, Ba, REEs (La, Ce, Pr, Nd), Th and U (Table 3). Barium concentration is of the order of 63%. However, visual inspection of the respective spectrum (not shown) does not reveal the presence of barium x-ray lines. Titanium, according to the results in the Table 3, is below the limit of detection and the error of analysis is very high (~ 22.3 wt%).

PIXE identified the presence of Al, Si, P, S, K, Ca, Ti, Cr, Mn, Fe, Zn, Y, Zr, Nb, Sn, Hf, Ta, Pt and Th (Table 4). Ti concentration exceeds 14 wt%.

4 Discussion

It should be noted that, due to high inhomogeneity of samples and small analysed volumes by each method, the comparisons between techniques should be treated with caution. It is very likely that every method analysed different parts of the field-collected sample material. The results should be treated as the first sign of presence of certain elements, rather than the definite quantitative indicator for the whole sampled areas. Overall, a range of elements of high economic value has been identified.

Table 3. Elemental concentrations obtained using the portable XRF analyzer: Mining mode of operation.

	A1		B1		B2		D1	
Element	**Conc. (%)**	**Error (%)**	**Conc. (%)**	**Error (%)**	**Conc. (%)**	**Error (%)**	**Conc. (%)**	**Error (%)**
Mg	< LOD	1.055	< LOD	0.892	< LOD	4.071	< LOD	8.133
Al	0.323	0.134	1.12	0.217	0.777	0.348	1.286	0.759
Si	13.378	0.557	6.383	0.437	11.118	1.532	6.228	1.548
P	< LOD	0.071	< LOD	0.425	< LOD	1.532	< LOD	2.164
S	< LOD	0.024	< LOD	0.049	< LOD	0.282	< LOD	0.268
Cl	0.02	0.012	< LOD	0.018	< LOD	0.032	0.119	0.052
K	< LOD	0.549	< LOD	1.058	< LOD	2.87	< LOD	5.913
Ca	< LOD	0.25	< LOD	0.437	< LOD	1.274	< LOD	2.694
Ti	< LOD	1.306	< LOD	2.713	< LOD	13.847	< LOD	22.281
V	< LOD	1.013	< LOD	1.752	< LOD	6.165	< LOD	12.033
Cr	< LOD	0.239	< LOD	0.432	< LOD	1.553	< LOD	3.27
Mn	< LOD	0.076	< LOD	0.125	0.332	0.173	0.593	0.334
Fe	1.633	0.059	5.733	0.137	9.641	1.522	18.015	3.208
Co	< LOD	0.024	< LOD	0.051	< LOD	0.092	< LOD	0.161
Ni	< LOD	0.01	< LOD	0.018	0.063	0.031	0.065	0.039
Cu	< LOD	0.004	< LOD	0.008	0.316	0.059	0.106	0.032
Zn	< LOD	0.005	< LOD	0.004	0.052	0.015	0.06	0.018
As	< LOD	0.002	< LOD	0.002	0.017	0.007	< LOD	0.009
Se	< LOD	0.002	< LOD	0.002	< LOD	0.011	< LOD	0.007
Rb	< LOD	0.002	< LOD	0.002	< LOD	0.003	< LOD	0.004
Sr	< LOD	0.002	0.002	0.001	< LOD	0.003	< LOD	0.003
Y	0.002	0.001	0.025	0.002	0.14	0.017	0.052	0.008
Zr	0.045	0.002	0.516	0.013	14.711	1.444	5.615	0.556
Nb	0.007	0.001	0.068	0.003	1.421	0.137	0.579	0.058
Mo	< LOD	0.002	0.006	0.002	0.04	0.018	0.019	0.012
Ag	< LOD	0.002	< LOD	0.002	< LOD	0.014	< LOD	0.009
Cd	< LOD	0.003	< LOD	0.004	< LOD	0.01	< LOD	0.013
Sn	0.018	0.004	0.013	0.005	0.721	0.085	0.977	0.108
Sb	< LOD	0.005	< LOD	0.006	< LOD	0.018	< LOD	0.022
I	< LOD	0.008	< LOD	0.009	< LOD	0.042	< LOD	0.073
Ba	< LOD	0.012	0.021	0.012	< LOD	0.076	0.082	0.054
Bal	84.391	0.19	85.857	0.23	59.014	1.979	62.623	1.565
La	< LOD	0.017	0.029	0.017	0.098	0.066	0.241	0.085
W	0.031	0.01	< LOD	0.028	0.187	0.057	< LOD	0.078
Au	< LOD	0.002	< LOD	0.004	< LOD	0.015	< LOD	0.016
Pb	< LOD	0.002	0.004	0.002	0.102	0.024	< LOD	0.03
Bi	< LOD	0.004	< LOD	0.009	0.133	0.052	< LOD	0.071
Ce	0.026	0.013	0.041	0.019	0.271	0.09	0.281	0.104
Pr	0.025	0.015	0.049	0.022	< LOD	0.173	0.254	0.107
Nd	0.032	0.02	0.078	0.031	< LOD	0.258	0.423	0.156
Th	0.002	0.001	0.011	0.003	0.679	0.075	0.299	0.04
U	< LOD	0.002	< LOD	0.002	0.036	0.006	0.013	0.003

Table 4. Average PIXE elemental concentrations for the scanned areas (A1 – 875 x 609; B1 – 861 x 602; B2 – 832 x 574; D1 – 861 x 602 all in μm). Spectra fitted using GeoPIXE software (Ryan et al. 2001)

	A1				B1			
Element	**Conc. (ppm)**	**Uncert (ppm)**	**MDL (ppm)**	**Rel. Error**	**Conc. (ppm)**	**Uncert. (ppm)**	**MDL (ppm)**	**Rel. Error**
Al	31868	2252	587	0.071	158905	7803	1381	0.049
Si	347480	1924	79	0.006	293510	7905	308	0.027
P	-	-	-	-	139	133	120	
S	110	26	48	0.241	-	-	-	-
K	509	23	15	0.045	3303	94	19	0.028
Ca	54	7	11	0.128	753	23	14	0.03
Ti	1472	57	8.4	0.039	7288	197	10	0.027
Cr	78	4	6.3	0.054	112	7	7.4	0.067
Mn	-	-	-	-	271	20	11	0.075
Fe	13574	289	6.1	0.021	66233	676	8.4	0.01
Ni	-	-	-	-	31	10	16	0.314
Zn	-	-	-	-	21	7	16	0.362
Y	-	-	-	-	76	19	34	0.247
Zr	162	31	69	0.189	6060	246	45	0.041
Nb	-	-	-	-	51	23	50	0.45
Sn	-	-	-	-	-	-	-	-
Sn L	-	-	-	-	-	-	-	-
Yb L	-	-	-	-	-	-	-	-
Hf L					272	28	39	0.102
Ta L	-	-	-	-	-	-	-	-
W L	205	17	36	0.083	-	-	-	-
Pt L	-	-	-	-	-	-	-	-
Au L	-	-	-	-	-	-	-	-
Th L	-	-	-	-	-	-	-	-
Th M	-	-	-	-	-	-	-	-
U L	-	-	-	-	-	-	-	-

	B2				D1			
Element	**Conc. (ppm)**	**Uncert. (ppm)**	**MDL (ppm)**	**Rel. Error**	**Conc. (ppm)**	**Uncert. (ppm)**	**MDL (ppm)**	**Rel. Error**
Al	23347	2305	1321	0.099	43190	2024	3756	0.047
Si	261792	5568	193	0.021	178365	3610	480	0.02
P	26901	3583	145	0.133	16828	3716	221	0.221
S	1111	602	69	0.542	2395	677	106	0.283
K	-	-	-	-	2766	174	32	0.063
Ca	152	82	15	0.54	532	46	24	0.087
Ti	41395	494	11	0.012	143892	3011	21	0.021
Cr	168	12	8.8	0.069	60	16	23	0.258
Mn	2044	61	11	0.03	7767	238	34	0.031
Fe	65895	759	10	0.012	169770	2860	31	0.017
Ni	-	-	-	-	-	-	-	-
Zn	495	40	29	0.081	709	79	65	0.112
Y	808	157	93	0.194	1747	125	159	0.071
Zr	120588	2975	128	0.025	108663	2215	220	0.02
Nb	15269	538	145	0.035	30368	522	232	0.017
Sn	3880	250	196	0.064	979	224	356	0.229
Sn L	2357	336	67	0.143	-	-	-	-
Yb L	404	103	66	0.255	-	-	-	-
Hf L	7907	264	63	0.033	6928	709	147	0.102
Ta L	1128	127	68	0.112	1153	314	155	0.272
W L	-	-	-	-	-	-	-	-
Pt L	585	158	69	0.27	1806	692	168	0.383
Au L	240	75	62	0.311	<237.	237	154	-
Th L	7503	531	105	0.071	15508	1400	241	0.09
Th M	2020	258	75	0.128	1723	245	131	0.142
U L	670	252	97	0.377	-	-	-	-

The portable XRF analyzer was used in laboratory conditions, while its main advantage is possibility of in-situ field analysis, on the mining sites. The calculation algorithm used in this analyzer assumes that the concentrations of detected elements should add up to 100%, without taking into account the not-detectable light elements, especially oxygen. Such approach leads to erroneous results, because in most cases the mineable elements are present in the oxide forms. Even worse problem was due to erroneous identification of Ti K-lines as Ba-L lines. This mistake was already easily seen upon visual inspection of the respective X-ray spectra. PIXE results gave an additional proof that barium results from XRF analysis were totally wrong. It should be stressed that PIXE is a more sensitive method and lower detection limits can be achieved for most elements, yet barium was never detected.

Comparison between the two methods, portable XRF and PIXE, leads to the conclusion that XRF results cannot be assumed to be quantitative and even qualitative results should be treated with caution and need confirmation by a laboratory method, such as PIXE. On the other hand, very fast XRF analyses can definitely be used as the first sign of a possible presence of elements of high economic value.

The capability to generate quantitative elemental maps, a very powerful feature of micro-PIXE, cannot be used properly when analyzing pelletized powders, as is the case here. Although the obtained maps (Figure 4) complement the average concentrations of elements within the scanned area, they merely show that the samples were not properly

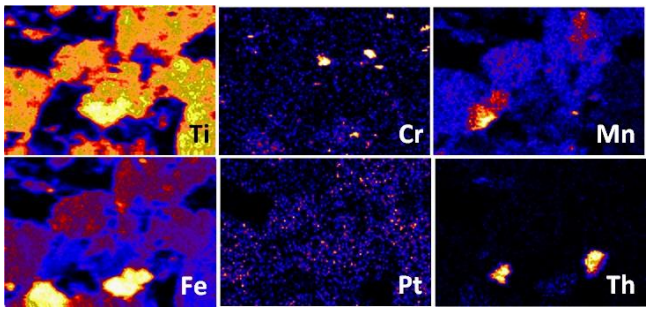

Figure 4: PIXE elemental distribution maps of sample D1. Maps (D1 – 861 x 602 μm) were generated using the Dynamic Analysis method.

5 Conclusions

The morphology and elemental characterization of tin mine tailing from Jos area, Nigeria have been carried out by μ-PIXE, XRF, SEM-EDS and XRD techniques. The SEM and XRD results were complementary in providing information on mineral phases, enabling a more holistic overview of the mineralization process. The presence of ilmenite as shown by the SEM/XRD is usually used as an indicator for tracing provenance of the placer deposits, and this mineral indicates a granitic source. The micro-PIXE elemental concentrations data and their distribution provided worthful data for underlying geological analyses as well as the systematic search for crucial trace elements, which confirms the granitic source of cassiterite in the sediment.

Caution is required when using automated elemental analysis of the portable XRF instrument,of which user has no control. The obtained results must always be confirmed using anotheranalytical method.

Acknowledgements

The staffs of the MRD, iThemba LABS, Chemistry and Physics Departments of the University of the Western Cape, South Africa are appreciated for their support. In particular, Dr Remy Bucher is acknowledged for XRD identification of mineral phases. FS OLISE is grateful to TWAS-UNESCO for the associateship award and the IAEA for the partial financial support to the Ion Beam Analysis (IBA) 2013 Conference in Seattle, USA.

References

[1] M. Benzaazoua, P. Marion, A. Pinto, H. Migeon, F.E. Wagner, "Tin and indium mineralogy within selected samples from the NevesCorvo ore deposit (Portugal): a multidisciplinary study",Miner. Engr., 16, 129–1302, 2003.

[2] B. Klein, N.E.Altun, H. Ghaffari, M. Mcleavy, "A hybrid flotation–gravity circuit for improved metal recovery",Inter. J. Miner. Proc., 94, 159–165, 2010.

[3] G.L.Chen, D. Tao, H. Ren,F.F. Ji, J.K. Qiao, "An investigationof niobite flotation with octyldiphosphonic acid as collector"Inter. J. Miner. Proc., 76, 111–122, 2005.

[4] V. Rodriguez-Santiago, M.V. Fedkin, D.JWesolowski, J. Rosenqvist, "Electrophoretic study of the SnO2/aqueous solution interface up to 260C", Langmuir, 25, 8101–8110, 2009.

[5] A.K. Somarin, "Ore mineralogy and mineral chemistry of the Glen Eden Mo-W-Sn greisen-breccia system, eastern Australia", J. Miner. Petrol.Sci., 104, 339–355, 2009.

[6] K. Germann, V. Luders, D.A. Banks, K. Simon, "Late Hercynian polymetallic vein-type base-metal mineralization in the Iberian Pyrite Belt: fluid-inclusion and stable-isotope geochemistry (S–O–H–Cl)", Mineral. Deposita, 38, 953–967, 2003.

[7] E. Mamontov, L. Vlcek, D.J. Wesolowsk, P.T. Cummings, W. Wang, L.M. Anovitz, "Dynamics and structure of hydration water on rutile and cassiterite nanopowders studied by quasielastic neutron scattering and molecular dynamics simulations", J. Phys. Chem. C 111, 4328–4341, 2007.

[8] Y.W. Wang, J.B. Wang, L.J. Wang, Y.Z. Chen, "Tin mineralization in the Dajing tin polymetallic deposit, Inner Mongolia, China", J. Asian Earth Sci. 28, 320–331, 2006.

[9] S.H. Sie, "Nuclear microprobe in geological applications: Where do we go from here?",Nucl. Instr. Meth.B130, 592–607, 1997.

[10] M. Ahmed, "Analysis of geological samples by the micro-PIXE facility at KFUPM",J. Radioanal. Nucl.Chem. 265, 39–45, 2005.

[11] J.B. Wright, D.A. Hasting, W.B. Jones, H.R. Williams, "Geology and mineral resources of West Africa",George Allen and Uwin, London, 1985.

[12] F.S. Olise, O.K. Owoade, H.B. Olaniyi, "Radiological indices of technologically enhanced naturally occurring radionuclides: a PIXE approach",J. Radiol. Prot.31, 255–264, 2011.

[13] B.W. Robinson, E.H. Nickel, "A useful new technique for mineralogy: The vacuum mode of SEM operation",Amer. Mineral.64, 1322–1328, 1979.

[14] F.S. Olise, O.K. Owoade, H.B. Olaniyi, "An optimization of PIXE procedure for high-Z species in a lower Z matrix", Appl. Radiat. Isot.68, 1030–1034, 2010.

[15] C.G. Ryan, D.N. Jamieson, W.L. Griffin, G. Cripps, R. Szymanski, "The new CSIRO -GEMOC nuclear microprobe: first results, performance and recent applications",Nucl. Instr. Meth., B181, 12–19, 2001.

[16] C.G. Ryan, "Quantitative trace element imaging using PIXE and the nuclear microprobe",Inter. J. Imag. Syst. Techn.11, 219–230, 2000.

[17] M. Ogwuegbu, G. Onyedika, J. Hwang, A. Ayuk, Z. Peng, B. Li, "Mineralogical characterization of Kuru cassiterite ore by SEM-EDS, XRD and ICP techniques",J. Miner. Mat. Character.Engr. 10, 855–863, 2011.